Title

Immunomodulatory extracellular matrix hydrogel induces tissue regeneration in a model of partial glossectomy.

Authors

Zelus, Emma

Panduro, Aaron

Deshmukh, Isha

et al.

Publication Date

2024-08-01

DOI

10.1016/j.bioactmat.2024.05.001

Peer reviewed

Bioactive Materials 38 (2024) 528–539

Contents lists available at ScienceDirect

Bioactive Materials

journal homepage: www.keaipublishing.com/en/journals/bioactive-materials

Immunomodulatory extracellular matrix hydrogel induces tissue regeneration in a model of partial glossectomy

Emma I. Zelus [a,d], Aaron Panduro [a,d], Isha Deshmukh [a,d], Jacqueline Grime [a,d], Marianna Alperin [b,d], Andrew M. Vahabzadeh-Hagh [c,**], Karen L. Christman [a,d,e,*]

[a] Shu Chien-Gene Lay Department of Bioengineering, UC San Diego, 9500 Gilman Dr. MC 0412, La Jolla, CA, 92093-0412, USA
[b] Department of Obstetrics, Gynecology, and Reproductive Sciences, Division of Female Pelvic Medicine and Reconstructive Surgery, UC San Diego School of Medicine, 9300 Campus Point, MC 7433, La Jolla, CA, 92037-7433, USA
[c] Department of Otolaryngology – Head & Neck Surgery, UC San Diego School of Medicine, 9300 Campus Point, MC 7400, La Jolla, CA, 92037-7400, USA
[d] Sanford Consortium for Regenerative Medicine, 2880 Torrey Pines Scenic Drive, La Jolla, CA, 92037, USA
[e] Sanford Stem Cell Institute, 2880 Torrey Pines Scenic Drive, La Jolla, CA, 92037, USA

ARTICLE INFO

Keywords:
Extracellular matrix
Biomaterial
Hydrogel
Skeletal muscle regeneration
Partial glossectomy
Dysphagia
Immunomodulation

ABSTRACT

While oropharyngeal cancer treatment regimens, including surgical resection, irradiation, and chemotherapy, are effective at removing tumors, they lead to muscle atrophy, denervation, and fibrosis, contributing to the pathogenesis of oropharyngeal dysphagia – difficulty swallowing. Current standard of care of rehabilitative tongue strengthening and swallowing exercises is ineffective. Here, we evaluate an alternative approach utilizing an acellular and injectable biomaterial to preserve muscle content and reduce fibrosis of the tongue after injury. Skeletal muscle extracellular matrix (SKM) hydrogel is fabricated from decellularized porcine skeletal muscle tissue. A partial glossectomy injury in the rat is used to induce tongue fibrosis, and SKM hydrogels along with saline controls are injected into the site of scarring two weeks after injury. Tissues are harvested at 3 and 7 days post-injection for gene expression and immunohistochemical analyses, and at 4 weeks post-injection to evaluate histomorphological properties. SKM hydrogel reduces scar formation and improves muscle regeneration at the site of injury compared to saline. SKM additionally modulates the immune response towards an anti-inflammatory phenotype. This study demonstrates the immunomodulatory and tissue-regenerative capacity of an acellular and minimally invasive ECM hydrogel in a rodent model of tongue injury.

1. Introduction

Dysphagia is a debilitating condition defined broadly as difficulty swallowing. Dysphagia may result from atrophy, denervation, or fibrosis of the tongue muscles [1]. While this condition is commonly implicated in aging or neurological disorders, another patient population of interest is those recovering from head and neck cancer [2]. Treatment of these cancers typically involves surgical removal of the tumor followed by radiation with or without chemotherapy. Dysphagia is a common sequela of treatment – affecting at least half of oropharyngeal cancer patients – and demonstrates a particularly high incidence following treatment of tongue cancer, which is the most frequent intraoral head and neck cancer [3,4]. Dysphagia is a morbid condition that severely affects quality of life and potentially leads to feeding tube dependence, aspiration, malnutrition, and even death [4,5]. Current standard of care for oropharyngeal dysphagia is limited to rehabilitative strategies such as swallow therapy and lingual muscle exercises. However, these approaches do not provide long-term improvement in swallowing and tongue strength, and they do not reverse the tissue-level pathology by improving muscle regeneration and reducing scar tissue formation [6]. About 18,000 cases of tongue cancer are diagnosed annually in the US, with a 5-year survival rate of approximately 70 %; as such, there is a growing patient population in dire need of improved treatment options following cancer treatment to prevent or reverse tongue fibrosis and atrophy and address the underlying pathophysiology of oropharyngeal dysphagia to not only prolong life but improve its quality.

Peer review under responsibility of KeAi Communications Co., Ltd.
* Corresponding author. Shu Chien-Gene Lay Department of Bioengineering, UC San Diego, 9500 Gilman Dr. MC 0412, La Jolla, CA, 92093-0412, USA.
** Corresponding author.
E-mail addresses: avahabzadehhagh@health.ucsd.edu (A.M. Vahabzadeh-Hagh), kchristman@ucsd.edu (K.L. Christman).

https://doi.org/10.1016/j.bioactmat.2024.05.001
Received 11 September 2023; Received in revised form 1 May 2024; Accepted 1 May 2024

Considering these deficiencies in treatment, a number of investigative cell-based therapies that seek to regenerate tongue muscle or provide structural augmentation to improve tongue function have emerged. While preclinical investigation of allogeneic mesenchymal stem cell injection in an athymic rat model has demonstrated some potential [7,8], the manufacturing, cost, and difficulties associated with a living stem cell product pose translational challenges. Additionally, autologous muscle-derived cell therapy demonstrated safety but lacked efficacy after 2 years in a Phase 1 trial [9]. Overall, the current body of research demonstrates a continued need for an accessible and minimally invasive therapeutic that can induce tissue regeneration to reduce scar formation and muscle atrophy to improve muscle repair and maintain muscle bulk.

The use of decellularized extracellular matrix (ECM) hydrogels that induce immune modulation, cellular recruitment and differentiation, neovascularization, and ECM remodeling has been explored as a therapeutic in numerous disease phenotypes [10]. The ECM is a complex network of proteins and polysaccharides vital for structural support and cell signaling; when a whole tissue is decellularized, the ECM remains as an acellular biomaterial with tissue regenerative properties [10]. Additionally, due to their thermoresponsive properties, ECM hydrogels, formed via partial enzymatic digestion of decellularized ECM, can be delivered minimally invasively via injection, and after exposure to physiologic conditions, the liquid forms a scaffold comprised of a nanofibrous ECM network [11]. With sufficient decellularization, the acellular xenogeneic ECM hydrogels are biocompatible and have been utilized in large [12,13] and small animal models [14], as well as a human Phase 1 clinical trial that assessed safety and feasibility for intervention in subacute and chronic myocardial infarction [15]. We have previously demonstrated that a decellularized porcine skeletal muscle ECM hydrogel (SKM) increased vascularization, enhanced the recruitment and differentiation of muscle progenitors, and reduced muscle atrophy and cell death in an ischemic injury model [11,16,17]. SKM has further been shown to prevent skeletal muscle atrophy and mitigate fibrotic degeneration, as well as modulate the immune response after mechanical muscle injury in pelvic floor muscles [18].

In the present study, we investigated the therapeutic efficacy and potential mechanisms of action of SKM in a preclinical animal model of partial glossectomy. We observed that SKM reduces scar formation and improves fiber area in a rat tongue partial glossectomy model. We further demonstrated that SKM modulates the immune response and upregulates genes related to angiogenesis. Overall, we found that SKM injection is a promising treatment in a preclinical model of partial glossectomy that warrants further investigation as a potential minimally invasive acellular therapeutic for oropharyngeal dysphagia.

2. Results

2.1. Determining optimal injection volume of SKM hydrogel

Acellular biomaterial therapeutics have not been previously investigated for oropharyngeal dysphagia in a pre-clinical animal model, so we first conducted a study to determine the optimal injection volume of SKM. A rat partial glossectomy injury model, previously developed to mimic the fibrosis and muscle atrophy that follows head and neck cancer treatment, was used [8]. The study design (Fig. 1A) included injection volumes ranging from 50 to 300 μL.

Based on previous ECM hydrogel studies, greater material retention led to improved repair with a typical degradation time of approximately 3 weeks; thus, it was desirable to see high material retention in the tissue at 1 week post-injection to enable prolonged pro-regenerative cues and sufficient repair [16,19]. Representative images of injection boluses are shown for all SKM dosages (Fig. 1B–E), demonstrating increased material retention and spread through the tongue with higher injection volumes. Therefore, we found that 200 and 300 μL injection volumes were suitable for further investigation.

2.2. Higher volume of SKM hydrogel reduces scar formation in a rat model of partial glossectomy

To investigate therapeutic potential of SKM hydrogel, the chosen

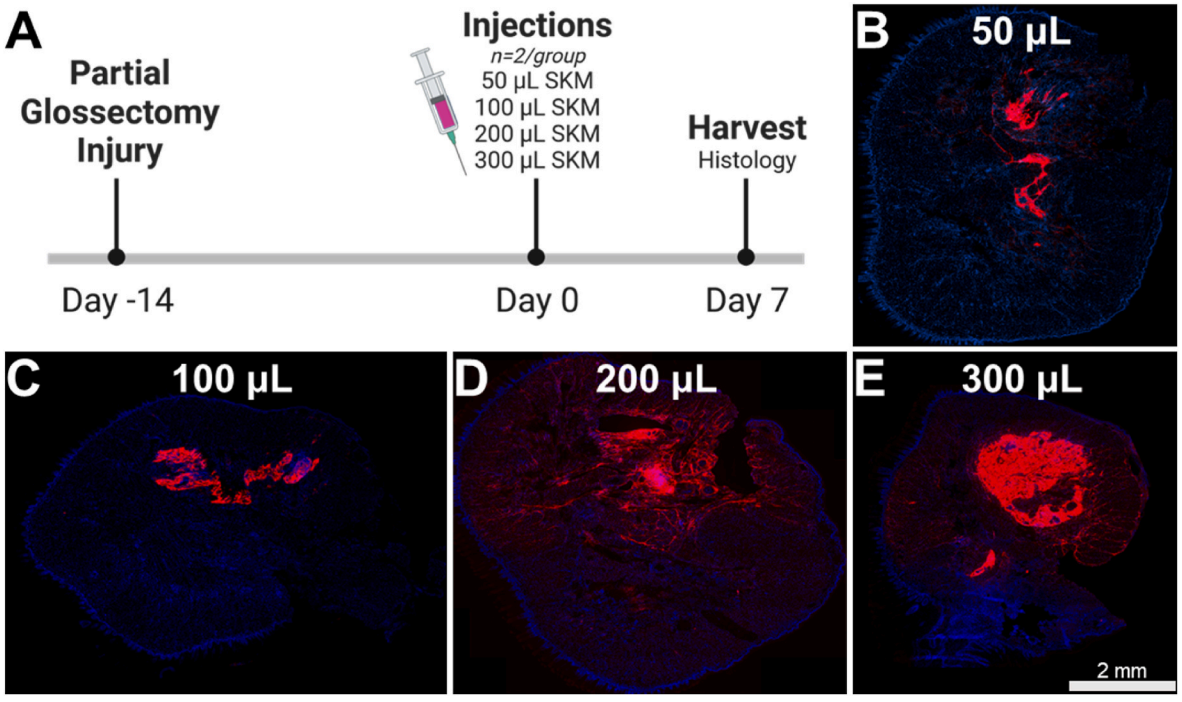

Fig. 1. SKM hydrogel injection volume optimization after tongue partial glossectomy injury. (A) A range of SKM volumes were injected 2 weeks after partial glossectomy injury, and tissues were harvested 1 week post-injection. Representative fluorescent images show pre-labeled SKM material in red against a DAPI counterstain in blue to indicate cell nuclei. SKM material spread and retention in the target tissue is shown for a range of injection volumes including 50 (B), 100 (C), 200 (D), and 300 μL (C). Scale bar: 2 mm.

injection volumes – 200 and 300 μL – were injected 2 weeks following partial glossectomy injury as low or high dose therapeutic options (Fig. 2A). The experimental control group received a saline injection at the same time point. Whole tongues were harvested 4 weeks after injection for assessment of histomorphological properties. First, we investigated whether SKM decreased scar formation in this injury model, which is important as scarring contributes to dysphagia following surgical resection of head and neck cancers. Representative brightfield images of tongue cross-sections from the treatment groups are shown in Fig. 2C–E. As shown in Fig. 2B, the scar area fraction was significantly reduced in the higher dose SKM group compared to both low dose SKM ($P = 0.005$) and saline ($P = 0.02$) groups.

2.3. SKM hydrogel improves muscle regeneration within scar region

For subsequent evaluation, only the higher dose SKM group was used, as the lower dose SKM injection did not demonstrate reduction of scar formation. Short axis cross-sections of tongue specimens were stained with antibodies against collagen I, sarcolemma (α-sarcoglycan), and a nuclear stain (DAPI). Representative fluorescent images are shown in Fig. 3A and B. A higher magnification image demonstrates the presence of skeletal muscle fibers (red) inside the scar area (green, Fig. 3C and D). To assess the effect of SKM injection on muscle regeneration, we quantified fiber number and fiber cross-sectional area inside the scar region, as defined by the area with collagen staining. There were no quantitative differences in myofiber density in the scar between the groups (Fig. 3E, $P = 0.86$), however, fiber cross-sectional area was significantly greater in the high dose SKM compared to saline group (Fig. 3F, $p < 0.0001$). Although, both SKM and saline demonstrated smaller fiber area compared to age-matched healthy controls (Figs. S1–C). The proportion of centrally nucleated fibers was quantified to determine if the muscle was actively regenerating; there was no difference between SKM and saline treated animals, indicating that muscle regeneration was not ongoing and fiber area measurements were reflective of the tissue at homeostasis. This was supported by comparison to central nucleation in healthy tissue (Fig. S1D), which showed no difference in proportion of centralized nuclei among SKM, saline, and healthy groups, indicating that both injected groups had returned to baseline and were not undergoing active regeneration.

2.4. SKM hydrogel upregulates pro-regenerative immune response, myogenic response, and angiogenic signaling

Having demonstrated significant histomorphological improvements with SKM injection in this model, we then conducted a gene expression study to investigate potential mechanisms driving these changes. Two weeks following partial glossectomy injury, SKM or saline were injected into the site of injury. Additionally, non-injected injured animals were used as controls. To capture physiologically relevant timepoints for early changes in the immune response, myogenesis, and ECM remodeling, tissues were harvested for RNA isolation at 3 and 7 days post-injection (Fig. 4A). A custom NanoString multiplex gene expression panel of 145 genes for rat skeletal muscle, which included pathways of interest such as the immune response, myogenesis, muscle anabolism/catabolism, angiogenesis, and ECM remodeling, was used to characterize the tissue response to injury with and without SKM injection (Table S1). The significantly differentially expressed genes for comparisons between SKM and either saline or no injection groups are shown for days 3 and 7 post-injection in Fig. 4B–E.

At day 3 post-injection, SKM induced dramatic differential gene expression as compared to non-injected controls. Genes involved in skeletal muscle structure and contraction were downregulated (*Acta1, Actn2, Des, Mybpc1, Mybpc2, Myf6, Myh1, Mylk2, Sln, Ttn3, Ttn*), as were genes related to muscle catabolism and cellular survival (*Akt2, Ccn4, Fbxo32, Nfkbia, Nol3, Rps6Ka1, Trim63*). Genes involved in ECM deposition and fibrosis (*Ctgf, Smad3, Timp1, Tgfb)* were upregulated, while some angiogenic growth factors (*Fgf2, Vegfb*). Several pro-inflammatory cytokines and chemokines (*Il1b, Il6, Il12b, Ccl2, Ccl3, Ccl4),* which are involved in early stage of injury response and facilitate recruitment of macrophages and neutrophils [20,21], were upregulated. SKM further demonstrated increased expression of *Irf4* and *Irf5* (transcription factors of M2 and M1 macrophages, respectively), *Il10ra* (implicated in the

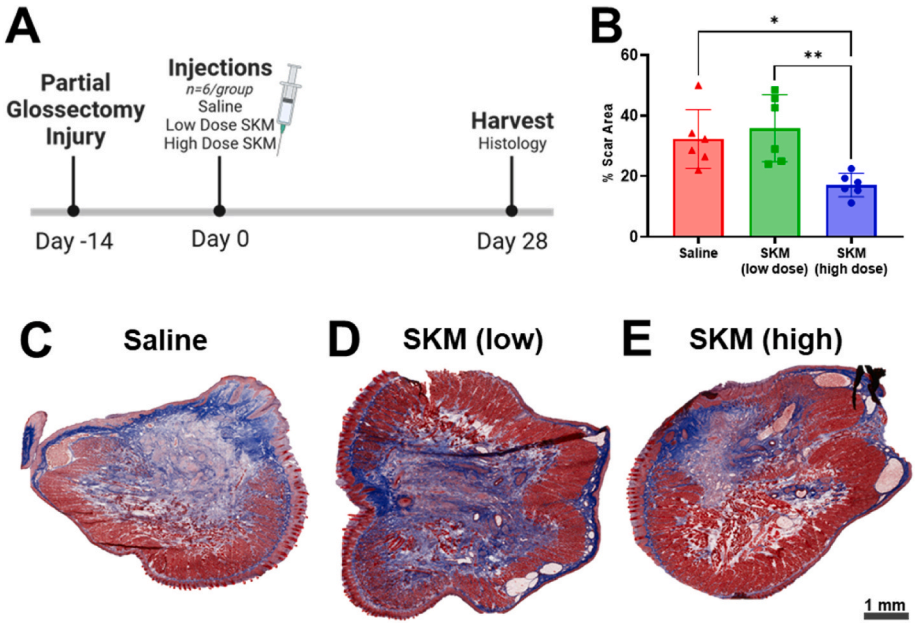

Fig. 2. SKM injection after partial glossectomy injury reduces scar formation. (A) Timeline of study to assess therapeutic potential of two doses of SKM hydrogel injection. Tissues were harvested 4 weeks after injection for assessment of scar formation via Masson's Trichrome stain, in which collagen is blue, denoting the scar region, and muscle fibers are red. (B) High dose SKM group significantly reduced scar formation compared to both the low dose SKM and saline injected groups. Treatment groups were compared using one-way ANOVA with Tukey multiple comparisons test (*$p < 0.05$; **$p < 0.01$). Representative images for the saline (C), low dose SKM (D), and high dose SKM (E) injection treatment groups are shown (Scale bar: 1 mm). Scar area was quantified and normalized to the total cross-sectional area for each tissue section including scar tissue, and values for all sections including the scar were averaged for each animal. n = 5–6 animals analyzed/group.

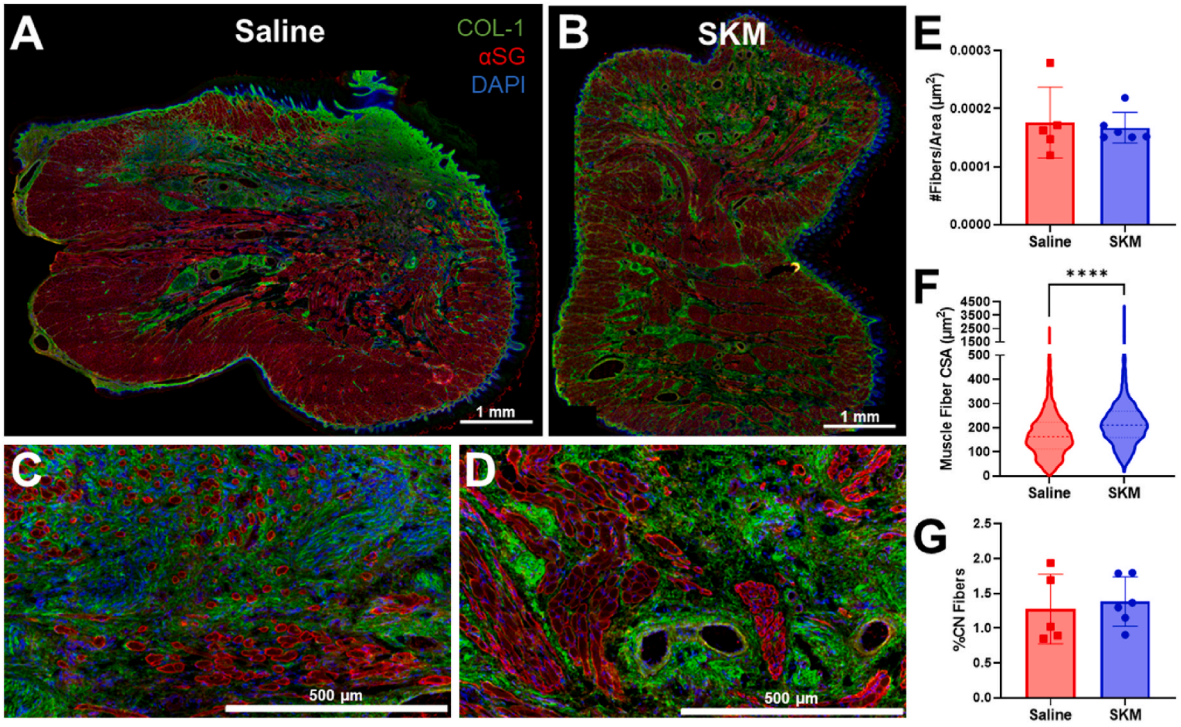

Fig. 3. SKM Injection improves muscle regeneration within scar area. Tongue sections underwent immunohistochemical staining to denote the scar (collagen I, green), myofibers (α-sarcoglycan, red), and nuclei (DAPI, blue). Representative fluorescent images are shown for saline (A) and SKM (B) injection groups (Scale bar: 1 mm). Higher magnification saline (C) and SKM (D) representative images demonstrated differences in fiber size and organization within the region of scar (Scale bar: 500 μm). (E) Fiber counts were normalized to scar area, showing no significant difference between treatment groups. (F) Muscle fiber area distributions are displayed as violin plots, with the dashed line indicating the median. Using a Mann-Whitney test, SKM demonstrated significantly increased fiber areas compared to saline injection (****$p < 0.0001$). (G) Within the scar area, proportion of fibers with centralized nuclei did not differ between groups. n = 5–6 animals analyzed per group.

transition of macrophages from the M1 to M2 phenotype), *Nkg7* (T cell marker), and *Cxcl1* (recruits neutrophils and M2 macrophages) [22]. SKM injection also led to upregulation of *Pdgrfralpha,* a marker for fibroadipogenic progenitors (FAPs), in addition to the cytokines *Il15* and *Il33*. *Il15* is known to be a key regulator of FAPs, inhibiting fatty infiltration and promoting muscle regeneration, while *Il33* is involved in recruitment of T regulatory (Treg) cells, which are similarly important in regulation of FAPs to promote a muscle repair phenotype [23,24].

At day 7 post-injection, the differential gene expression between SKM and no injection groups altered significantly. Relative to day 3, fewer genes involved in muscle structure were downregulated (*Mstn, Myh1, Mypbc2, Tcap, Ttn)*, and other genes involved in muscle structure and myogenesis were indeed upregulated (*Hgf, Myh3, Myh7, Tnnt1*). At this timepoint, there was a general shift in ECM expression towards remodeling through the downregulation of MMP inhibitors (*Timp3, Timp4*) and the upregulation of MMPs (*Mmp2, Mmp9, Mmp12, Mmp14)*. There was persistent upregulation of some pro-inflammatory cytokines and chemokines (*Ccr2, Ccl2, Il12b*) and M1 macrophage transcription factors (*Irf5, Stat1*). Additionally, T cell marker *Nkg7* and, in particular, the Th2 marker *Gata3*, were both upregulated at this time point in the SKM group. Macrophage marker *Adgr1* was enriched, and several pro-regenerative cytokines (*Il10, Il10ra, Il15*) demonstrated increased expression at this timepoint as well.

The significant differentially expressed genes between SKM and saline animals are displayed in a volcano plot for days 3 and 7 post-injection alongside their associated pathways in Fig. 4D and E, respectively. At day 3 post-injection, SKM led to upregulation of *Adgr1*, a macrophage marker, as well as *Pparg*, a macrophage transcriptional marker of pro-repair macrophages [25]. We further observed SKM immunomodulation through the downregulation of *Cxcr2,* associated with neutrophils and a pro-inflammatory response, and upregulation of pro-regenerative cytokine *Il33* with respect to saline. SKM also resulted in upregulation of *Ctgf*, which is known for a pro-reparative role in wound healing when expressed transiently in early injury response [26]. Compared to saline, SKM group had higher expression of *Timp4*, a matrix metalloproteinase inhibitor that regulates ECM remodeling as well as angiogenesis [27].

At day 7 post-injection, SKM modulation of *Adgr1*, *Cxcr2,* and *Il33* expression was maintained with respect to saline. SKM induced downregulation of *Nfkbia*, which is an inhibitor of the NF-κB pathway. Finally, SKM increased expression of *Vegfr2* and downregulated *Thsb1*, indicating an overall increase in angiogenic signaling.

To confirm and further assess transcriptomic changes at these early timepoints, RNA from tissues collected 3 and 7 days post-injection for SKM, saline, and non-injected groups underwent bulk RNA sequencing. Differential expression at 3 (Fig. 5A) and 7 (Fig. 5B) days post-injection for SKM and non-injected groups based on this analysis is shown in volcano plots, alongside gene ontology for up- and downregulated genes at each timepoint in Fig. 5. At 3 days post-injection, SKM upregulated pathways were associated with muscle development and regeneration as well as blood circulation and vasculature development. Downregulated pathways of note included maintenance of keratinized epithelium (keratinocyte development and differentiation, formation of the cornified epithelium) and regulation of immune response (cytokine production, mast cell degranulation). Conversely, at day 7 post-injection, upregulated pathways are almost entirely related to immune activation and regulation.

Differential expression between SKM and saline was also evaluated at these timepoints. As fewer differentially expressed genes, genes were assessed individually rather than utilizing GO analysis, At both day 3 (Fig. 5C) and day 7 (Fig. 5D) post-injection, these genes were predominately associated with the immune response – particularly upregulation

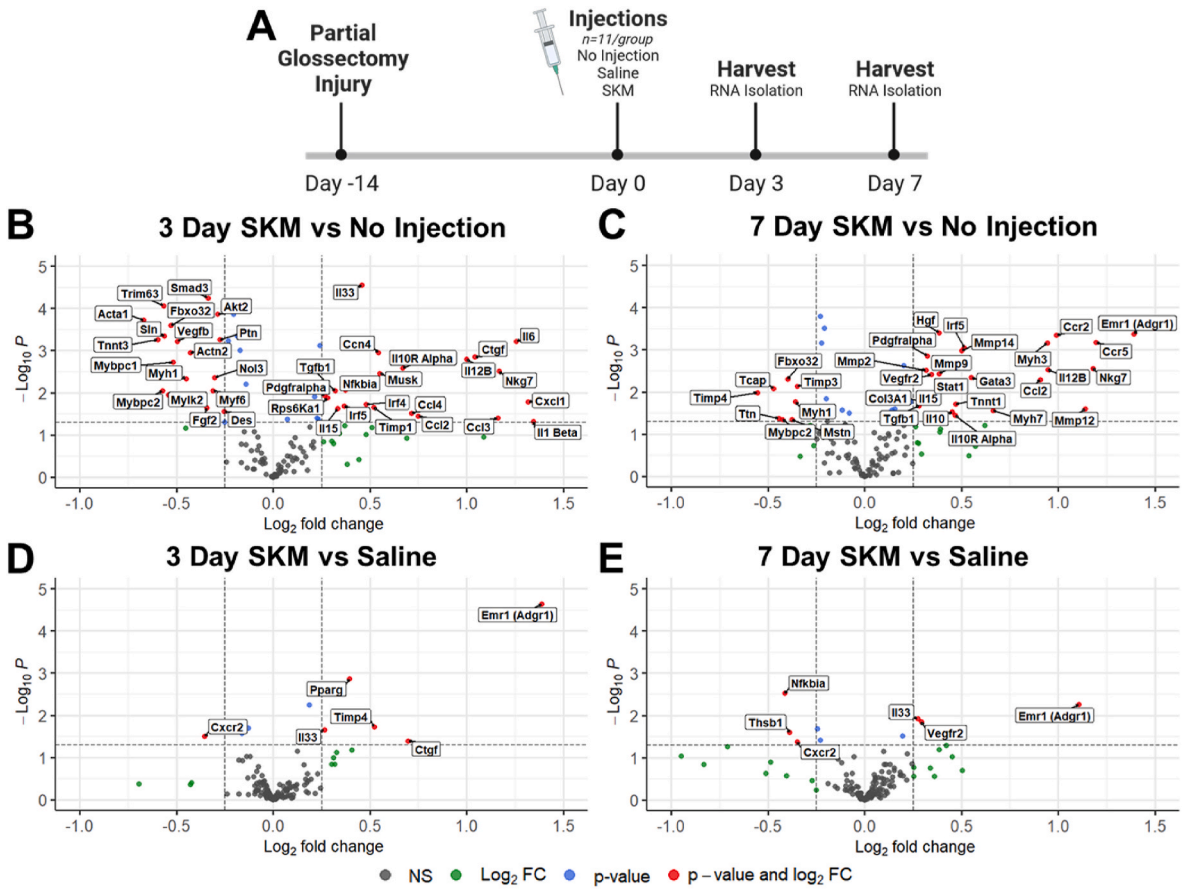

Fig. 4. SKM injection induces significant differential transcriptomic expression when compared to both no injection and saline control groups. (A) Experimental timeline for gene expression study using a custom NanoString multiplex gene expression panel. Differentially expressed genes between SKM and either no injection (B–C) or saline controls (D–E) are displayed in a volcano plot for both 3 and 7 day timepoints. n = 11 animals analyzed per group.

of immune cell infiltration (*Ccr9, Ddx60, Pla2g2d, Pdia5*), Treg response (*Ly49si4, Rsad2, Slc13a3, Xcr1*), macrophage response (*Adgre1, Pdia5, Slc13a3*), regulation of the immune response (*Klf2, Lgals9*), and other immune related or interferon induced genes (*Jchain, RGD1563231, Fclr2, Mx2, C6, Cmpk2, Gbp1, Gbp6-ps2*) as well as downregulation of pro-inflammatory expression (*Defb4, Rpph1, Slc15a1*) and genes that inhibit T-cell and macrophage activity (*Klk12, Vsig10l, Tmem125*). We additionally observed upregulation of genes supporting myoblast differentiation and regeneration (*Per1, Oas1f, Oas2*) and proliferation (*Egr1*). Finally, genes involved in keratinization and cornified envelop development were downregulated (*Lce3d, Loricrin*).

2.5. SKM hydrogel promotes an increase in microvasculature development

Gene expression results from both NanoString and bulk RNA sequencing demonstrated upregulation in angiogenic signaling and vasculature development. To further investigate this, tissue sections were assessed for vasculature development 7 days post-injection of either saline or SKM since angiogenic signaling was observed at 3 days post-injection. Additionally, vasculature was assessed at 4 weeks post-injection. Tissue sections were stained against alpha smooth muscle actin and isolectin, and arteriole size and density were assessed throughout the tissue at the 7 day timepoint, as there was no clear scar delineation at this acute timepoint, and within the scar area at the 4 week timepoint. At 7 days post-injection, SKM demonstrated significantly higher vessel density (Fig. 6C) and a smaller size distribution of vessels (Fig. 6D). These trends were maintained at 4 weeks post-injection, but the difference in vessel density was no longer significant (Fig. 6E), while the difference in vessel size distribution was maintained (Fig. 6F).

2.6. SKM injection leads to increased fibroadipogenic progenitors at 3 days post-injection and encourages myogenic growth

FAPs – a population of mesenchymal stromal cells in the interstitial space [28] – appeared to be involved in the SKM response, based on the differential gene expression results shown above. Therefore, we assessed FAPs at 3 days post-injection within the area of injury, which was defined by disrupted muscle structure and hypercellularity. Tissue sections from saline and SKM groups were stained against PDGFRα, an established marker of FAPs [29], and α-sarcoglycan, a muscle membrane marker (Fig. 7A and B). Percentage of PDGFRα$^+$ cells (Fig. 7C), normalized to the total number of cells within the injured area, was compared between groups, and the SKM group demonstrated significantly increased proportion of these PDGFRα$^+$ cells (Fig. 7D). Additionally, PDGFRα$^+$ cells were observed infiltrating the SKM scaffold alongside myofibers (Fig. 7E and F). To further investigate whether FAPs were involved in mediating a SKM-driven pro-myogenic response, tissue sections were stained against embryonic myosin heavy chain, a well-established marker of developing myofibers. Embryonic myosin heavy chain positive fibers were observed localizing alongside FAP cells that had infiltrated the SKM scaffold (Fig. 7G and H).

2.7. SKM injection mitigates area of injury as early as 7 days post-injection

Given positive immune regulation and vasculature development

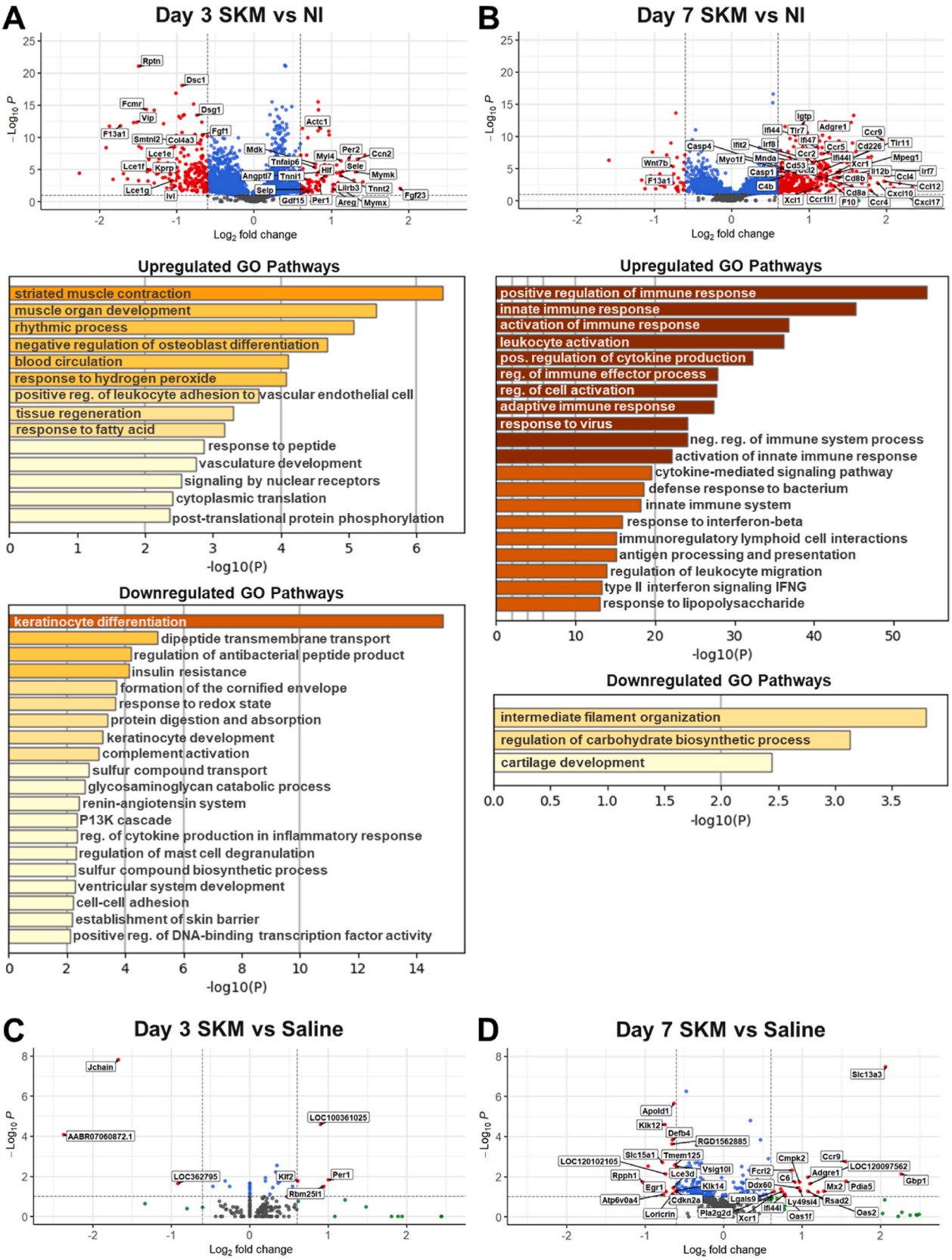

Fig. 5. SKM injection stimulates muscle regeneration and immune response related pathways and genes as demonstrated through differential bulk RNA sequencing analysis. RNA isolated from tongue tissues at day 3 and 7 post-injection of SKM or saline and non-injected tissues – previously used for NanoString multiplex gene expression analysis – underwent bulk RNA sequencing. Volcano plots of differentially expressed genes through comparison of SKM and non-injected tissues at day 3 (A) and day 7 (B) post-injection are shown, alongside their respective gene ontology pathways for up- and downregulated biological processes. Similar volcano plots for differential expression between SKM and saline injected time points at day 3 (C) and day 7 (D) post-injection are shown. n = 8 animals analyzed per group.

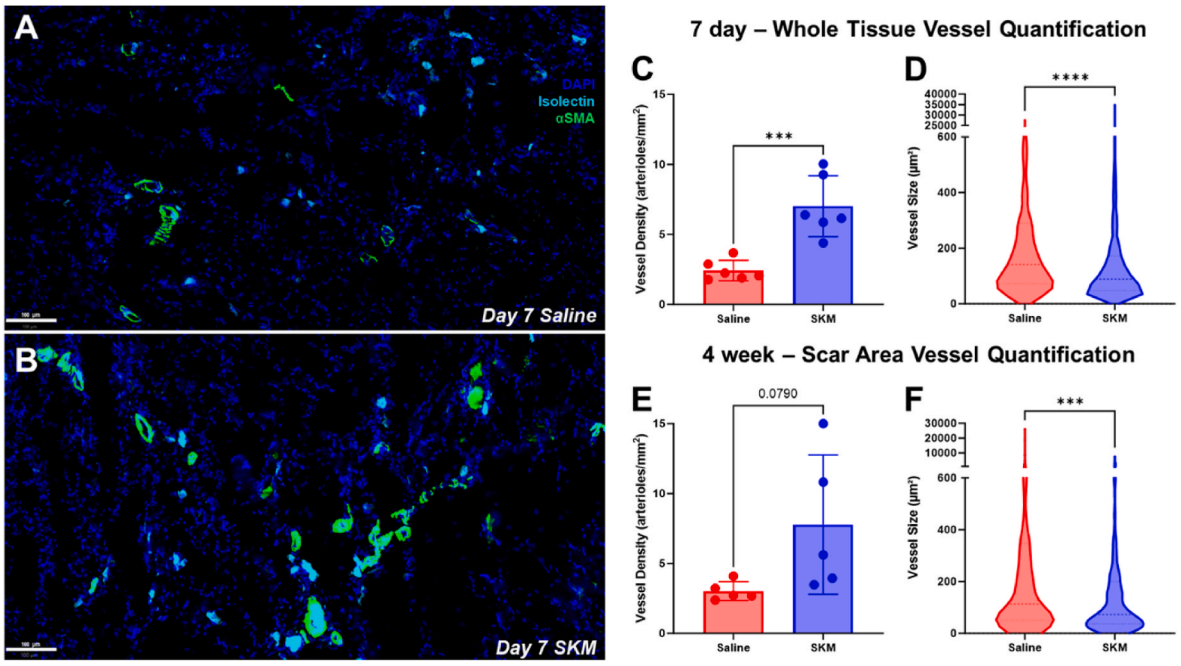

Fig. 6. SKM injection promotes a transient increase in vasculature development. Tissue sections were stained against smooth muscle (αSMA, green), endothelial cells (isolectin, cyan), and nuclei (DAPI). Arterioles, double positive for αSMA and isolectin, were counted and assessed for lumen area. Representative images of stained tissue from saline (A) and SKM (B) treated animals at 7 days post-injection are shown (Scale bar: 100 μm). (C) At 7 days post-injection, SKM group demonstrated significantly higher vessel density throughout the whole tissue section (unpaired *t*-test, ***p<0.001). (D) The vessels in SKM injected animals demonstrated a significantly smaller overall size distribution at 7 days post-injection (Mann-Whitney test, ****p<0.0001). (F) At 4 weeks post-injection, there was a nonsignificant increase in vessel density within the scar area in SKM injected animals (unpaired *t*-test, p=0.079). (F) At 4 weeks post-injection, the smaller size distribution of vessels in the SKM group was maintained (Mann-Whitney test, ***p<0.001). n = 6 animals per group.

gene expression signaling, as well as improved vascularization in the tissue 7 days post-injection of SKM, we investigated the development of tissue injury at 3 and 7 days post-injection. At these early timepoints, there is not a well-developed scar – instead, the injured area can be defined by damaged tissue and hypercellularity. Tissue morphology was assessed for these characteristics with a hematoxylin and eosin stain, and the region of injury was normalized to total tissue area. Representative tissue sections are shown for saline and SKM injected animals at 3 and 7 days post-injection (Fig. 8A–B, D-E). At 3 days, there was no difference in injured area between groups (Fig. 8C), but at 7 days post-injection, the SKM group demonstrated a decreased injured area compared to saline (Fig. 8F).

3. Discussion

SKM hydrogels have previously demonstrated induction of muscle regeneration, neovascularization, and ECM remodeling in several skeletal muscle conditions, including ischemia reperfusion [17] and birth-related mechanical injuries [18]. Thus, we hypothesized that injection of SKM hydrogel would mitigate scar formation and improve muscle regeneration in an animal model of partial glossectomy, which was previously developed to model pathologies associated with head and neck cancer treatment [8]. In this study, we demonstrated that injection of SKM two weeks following a partial glossectomy significantly improved histomorphological properties of the tongue. The active phase of muscle regeneration was completed 4 weeks after injection, as demonstrated by the proportion of muscle fibers with centralized nuclei in the site of injury returning to the healthy baseline [30], so this timepoint was used for evaluation of histomorphological changes in the tongue. At this timepoint, we found that 300 μL SKM injection reduced scar formation and improved muscle regeneration within the scar region. These data suggest therapeutic efficacy of SKM in promoting constructive remodeling and reversing fibrosis of the tongue consequent to surgical resection. Interestingly, a smaller injection volume of SKM did not significantly reduce scar area as compared to saline controls. This is likely due to the shorter retention time with the smaller volume, which was insufficient to induce a therapeutic effect and consequent histomorphological changes. We further assessed the area of injury at 3 and 7 days post-injection of 300 μL SKM or saline and found that SKM begins to mitigate the area of injury as early as one week post-injection, supporting the improved tissue regeneration outcomes we found at the 4 week timepoint.

Gene expression experiments revealed differences between SKM and non-injected control animals, which were greater than those between SKM and saline groups, which highlights the importance of saline injected control groups, as a significant muscle regeneration cascade can result from injection injury alone. However, we did still observe interesting differential gene expression between the SKM and saline injected groups. Consistent with previous studies on ECM hydrogels [18,31–33] we observed a strong macrophage response following SKM injection. Overall, SKM appears to modulate the injured tissue from pro-to anti--inflammatory immune phenotype; *Pparg* is particularly associated with muscle repair and M2 macrophages, while *Il33* is associated with Treg recruitment and muscle regeneration [28,34]. The gene expression data, comparing SKM injection to both saline and non-injected controls, suggested involvement of FAP activity as a potential mechanism by which SKM injection yields the observed improvements in muscle regeneration and reduction in scar formation. FAPs are known to be the primary muscle-resident producers of *Il33* in skeletal muscle, which was upregulated at both 3 and 7 days post-injection in the SKM groups [35]. We also found upregulation of *Pdgfra*, a marker of FAPs at both timepoints when comparing gene expression between SKM and non-injected animals. FAP activity was also supported by the transient upregulation of *Il6* at day 3 – a myogenic factor when expressed at early timepoints that is primarily produced by FAPs during muscle regeneration [28] – along with cytokines commonly implicated in the cross-talk between

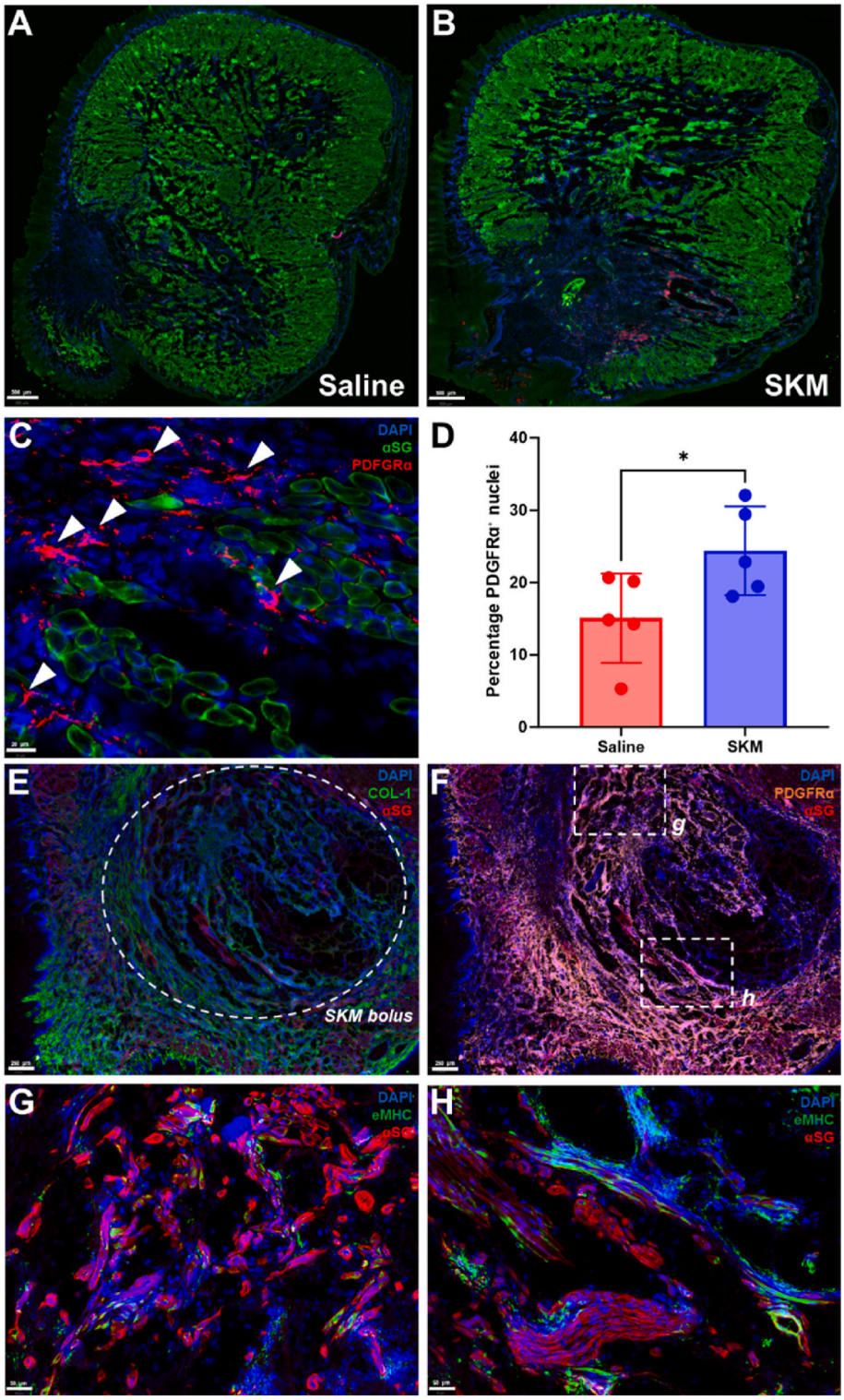

Fig. 7. Fibroadipogenic progenitors are more prominent in the SKM group 3 days post-injection and are colocalized with developing myofibers within the SKM scaffold. Tongue tissues harvested 3 days post-injection were stained against skeletal muscle (α-sarcoglycan, green), fibroadipogenic progenitors (PDGFRα, red), and nuclei (DAPI, blue) for both saline (A) and SKM (B) injection groups (Scale bar: 500 μm). PDGFRα⁺ nuclei (C, white arrows; Scale bar: 20 μm) within the area of injury were normalized to total nuclei within the injury, and SKM demonstrated an increased percentage of PDGFRα⁺ nuclei (D). SKM bolus was visualized with collagen staining (E, dashed oval), and PDGFRα⁺ nuclei (orange), representing fibroadipogenic progenitors, were observed infiltrating the SKM bolus (Scale bar: 250 μm). (G, H) Within the bolus, developing myofibers (embryonic myosin heavy chain, green) were observed in regions with high density of fibroadipogenic progenitors (Scale bar: 50 μm). n = 5 animals/group.

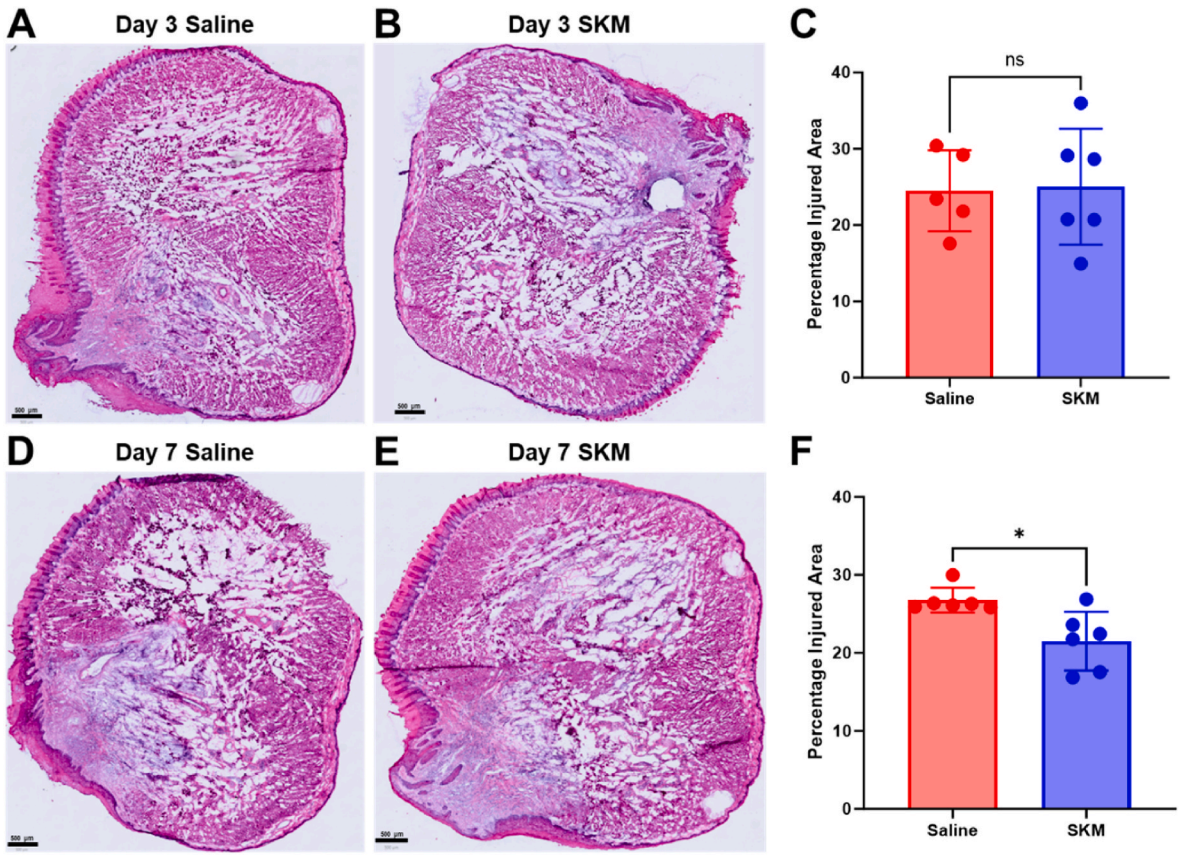

Fig. 8. SKM injection mitigates area of injury as early as 7 days post-injection. Tissue sections were stained against hematoxylin and eosin at the 3 day timepoint for saline (A) and SKM (B) treated animals (Scale bar: 500 μm). (C) There was no significant different in percentage of injured area between SKM and saline groups at 3 days post-injection. At the 7 day timepoint, representative images for saline (D) and SKM (E) are shown (Scale bar: 500μm). (F) At 7 days post-injection, SKM group demonstrated significantly reduced percentage of injured area (*t*-test, *$p<0.05$). n = 6 animals per group.

FAPs, macrophages, Tregs, and muscle stem cells (*Il10, Il15)* [36,37]. To support these gene expression data, we demonstrated a significant increase in FAP cell density within the area of injury in the SKM group compared to saline at the 3 day timepoint. Additionally, we found that FAPs are recruited to the SKM bolus alongside newly formed myofibers. While not observed in other injury models [17,18,38], SKM injection appears to repair the tongue tissue through FAP-mediated immunomodulatory activity in this injury model. Thus, the data presented here pose an exciting avenue for future research to investigate the precise interactions between ECM hydrogels, FAPs, immune populations, muscle stem cells, and myofibers. Additionally, we found that SKM injection upregulated genes involved in angiogenesis, which is consistent with our previous studies in which SKM induced neovascularization in other skeletal muscle injury models [17,19].

Results of bulk RNA sequencing affirmed many findings from the NanoString multiplex gene expression panel; when compared to non-injected controls, SKM injection led to significant immunomodulation as well as increases in muscle regeneration and vascularization. Comparison to saline controls revealed fewer differentially expressed genes, but expression was again consistent with previous results. Transcriptomic changes predominately involved the immune system – particularly mitigating pro-inflammatory expression and promoting activity of macrophages and Tregs. Additionally, we observed upregulation of genes involved in muscle regeneration and proliferation in the SKM injected group compared to saline controls, supporting the improved muscle regeneration observed 4 weeks post-injection. Supporting results from NanoString gene expression analysis and RNA sequencing demonstrated upregulation in vascularization, and indeed we found a transient increase in microvasculature development at the 7 day timepoint with SKM treatment.

One limitation of the partial glossectomy injury model is that while it induces muscle damage and scar formation that mimic the pathologies associated with head and neck cancer treatment, it does not include radiation. Additionally, while substantial histomorphological improvements were observed in both scar formation and muscle regeneration following SKM, we did not observe complete remission of the scar, and while muscle fibers within the scar were larger in the SKM group than saline, they did not return to healthy tongue muscle fiber area distribution. As such, it may be beneficial to investigate the therapeutic efficacy of repeated SKM injections in future studies. Finally, while our preliminary mechanistic insights from this study support the immunomodulatory effect of SKM, future studies utilizing flow cytometry would be valuable to differentiate and quantify changes in immune and muscle resident cell populations. Flow cytometry would additionally be helpful for further assessing the effect of SKM on FAPs, as using multiple markers to robustly identify this population is preferable to immunohistochemical staining.

Overall, the data support our hypothesis that SKM is a promising therapeutic for the treatment of fibrosis in the tongue. In this rat model of partial glossectomy, we demonstrate significant histomorphological improvements following SKM injection. Our gene expression data suggest immunomodulation towards a pro-regenerative phenotype. This study encourages further investigation of SKM for the regeneration of damaged tongue tissue for the potential treatment of dysphagia.

4. Conclusions

In conclusion, our study demonstrates that a cost-effective and easily

administered acellular tissue-specific biomaterial significantly reduces scar formation and improves muscle regeneration following partial glossectomy in a rat model. We provide evidence that this biomaterial is immunomodulatory and promotes a pro-reparative phenotype. Overall, this biomaterial, which can be delivered minimally invasively, presents a promising option for future clinical translation in the regeneration of tongue muscle and treatment of dysphagia.

5. Experimental section

5.1. SKM hydrogel fabrication

SKM material was fabricated as previously described [39]. Briefly, porcine skeletal muscle was chopped into small cubes before being spun in a 1 % sodium dodecyl sulfate detergent solution for 5 days, with daily solution changes. Tissue was thoroughly rinsed in water to remove residual detergent. Decellularized tissue was frozen at −80 °C and then lyophilized for 48 h, after which the material was milled to a fine powder. This powder was partially enzymatically digested at 10 mg/ml in pepsin (1 mg/mL pepsin in 0.1 M HCl) for 48 h, and then pH was neutralized and ionic concentration balanced. SKM was brought to a concentration of 6 mg/mL, which was previously determined as the optimal concentration for skeletal muscle injection [19].

5.2. Partial glossectomy model

All procedures were approved by the Institutional Animal Care and Use Committee at the University of California, San Diego. As oropharyngeal cancer is over twice as common in men than in women [40], male Sprague Dawley rats weighing between 225 and 250 g (approximately 3 months old) underwent partial glossectomy injury, as previously established [8]. Briefly, animals were anesthetized with isoflurane, and buprenorphine was delivered subcutaneously for pain management. The tongue was retracted out of the mouth with a 4–0 silk suture. A 4 mm dermal punch was used to standardize the volume of excised tongue. The dermal punch was applied to the left posterior quadrant of the tongue and inserted to a depth of 4 mm, leaving a thin layer of intact ventral tongue so that the defect was not through and through. The volume of removed tongue was placed on a sheet for visual confirmation of consistency between animals. Silver nitrate chemical cautery was used for hemostasis. The animals were then monitored for 5 days postoperatively; the rats were provided with a soft diet for the duration of the study period. Scar formation at the site of injury occurred over the following 2 weeks [8], at which time point SKM was injected directly into the tongue.

5.3. Reliability of the SKM injection and volume optimization

To enable visualization of SKM *in situ*, SKM was prelabeled with Alexa Fluor™ 568 NHS Ester (Thermo Fisher Scientific, Waltham, MA). SKM was incubated at room temperature for an hour to ensure complete binding. Fluorescently pre-labeled SKM was injected directly into the site of injury, two weeks following a partial glossectomy injury. Injection volumes of 50, 100, 200, and 300 μL were included (n = 2 animals per volume); this range was determined based on SKM injections in other skeletal muscle injury models [19] and cell injections in the rat tongue [8]. The rat tongue can only accommodate so much injectate before the tongue swells too much and injectate spills out of the injection site (backflow) once the needle is withdrawn. From our prior experience with an injectate of similar viscosity, 300 μL was determined to be an upper limit of injected volume for the adult rat tongue in this model. Animals were euthanized and tongues were harvested 1 week following injection; tissue was cryosectioned and stained with DAPI nuclear counterstain for tissue localization. Tissue cross-sections were then visualized at 20X magnification using a Leica Ariol® fluorescent microscope.

5.4. Histomorphological assessment of SKM therapeutic efficacy

5.4.1. Quantification of scar area

Two weeks following partial glossectomy injury, SKM or saline were injected into the injury site. Based on the injection volume optimization study, the 200 and 300 μL demonstrated good retention and spread in the tongue tissue. Thus, experimental groups included 200 μL SKM, 300 μL SKM, and 200 μL saline (n = 6/group). Animals were euthanized 4 weeks following injection and tongues were harvested and cryosectioned. Masson's Trichrome (Polysciences, Warrington, PA) stain was used to identify collagen and muscle, and tissue sections were visualized using a Leica Aperio ScanScope ® CS2. For quantification of the scar area from the Masson's Trichrome stained tissue sections, Aperio ImageScope software was used to trace the border of the scar region, as defined by the blue collagen stain. The outer edge of the tongue cross-section was traced, and the area of the scar was normalized to total tongue area for each section. All sections containing the scar were analyzed, and normalized scar area data were averaged per animal.

5.4.2. Quantification of muscle fiber area and centralized nuclei

For this analysis, age-matched healthy control animals were euthanized (n = 6) to assess muscle fiber area. For assessment of muscle regeneration within the scar area, fibrosis was identified with an anti-collagen I antibody (Bio-Rad, Hercules, CA, 1:200) with an Alexa Fluor™ 488 secondary (Invitrogen, Carlsbad, California, 1:500) secondary, and myofiber membranes were identified with anti-α-sarcoglycan antibody (Leica Biosystems, Wetzlar, Germany, 1:200) with an Alexa Fluor™ 568 secondary (Invitrogen, Carlsbad, California, 1:500). Tissue sections were visualized using a Leica Ariol® fluorescent microscope. For quantification of muscle fibers from immunohistochemical staining, the scar region (collagen I) and cross-sectional muscle fibers (α-sarcoglycan) within the scar region were identified, and myofiber cross-sectional areas were quantified. For healthy controls, sections were selected from the location in tongue where the scar was present in injured animals, and a circular region of interest was drawn in the left anterior tongue at these locations to match the site of injury (Fig. S1A). For the healthy animals, all muscle fibers within the selected region of interest were analyzed. Muscle fibers with centralized nuclei (DAPI) were also identified. Numbers of fibers were normalized to scar area, and the numbers of centrally nucleated fibers were normalized to muscle fiber counts within the scar. All sections containing scar were analyzed, and data were averaged per animal.

5.4.3. Quantification of arteriole density

For evaluation of vascularization, blood vessels were identified with a co-stain of an anti-αSMA antibody (Agilent, Santa Clara, California, 1:75) with an Alexa Fluor™ 568 secondary (Invitrogen, Carlsbad, California, 1:500) and anti-isolectin B4 antibody conjugated to fluorescein (Vector Laboratories, Newark, California, 1:75), alongside an anti-collagen I antibody with an Alexa Fluor™ 647 secondary (Invitrogen, Carlsbad, California, 1:500). Tissue sections were visualized using a Nikon Eclipse Ti2-E fluorescent microscope. For quantification of vessels, arterioles were identified by a positive co-stain of both αSMA and isolectin B4, and only arterioles with clearly defined and cross-sectional lumens were quantified. Arteriole density was quantified with respect to the scar area per tissue section, and arteriole lumen area was traced using the interior border of endothelial stain for each vessel. All tissue sections containing scar were analyzed, and data were averaged per animal.

5.5. RNA isolation, nanostring multiplex gene expression analysis, and bulk RNA sequencing

5.5.1. Study design and RNA isolation

Two weeks after partial glossectomy injury, either 300 μL of SKM or saline was injected into the injury site (n = 6/group). 300 μL injection

volume was chosen based on histological data, and the control saline injection was increased to 300 μL to match SKM. An injured non-injected group was used as an additional control to further evaluate potential effects of the injection itself. At 3 and 7 days post-injection, physiologically relevant timepoints for the immune response and early muscle regeneration, tongues were harvested and submerged in RNAlater™ (Thermo Fisher Scientific, Waltham, MA), then stored at 4 °C overnight before being transferred to −80 °C to preserve tissues for RNA isolation. For RNA isolation, tongue specimens were thawed and tissue was trimmed to isolate the scar region. Isolated scar region was divided in half, to accommodate spin column capacity, and homogenized (TissueRuptorII, Qiagen, Germantown, Maryland), and RNA was isolated with RNAeasy Fibrous Tissue Mini Kit following manufacturer instructions (Qiagen, Germantown, Maryland).

5.5.2. NanoString multiplex gene expression analysis

As previously described [18], we used a NanoString nCounter ® MAX Analysis System with an nCounter® custom CodeSet of 145 genes involved in pathways relevant to skeletal muscle regeneration [18]. Briefly, RNA concentration was measured using a Qubit 3.0 Fluorometer with a Qubit™ RNA HS Assay kit. The hybridization buffer (70 μL) was then mixed with the Custom Reporter CodeSet solution, and 8 μL of this master mix was then added to 50–100 ng of RNA per tissue sample, and RNA-free water up to 13 μL total. Then, 2 μL of Capture ProbeSet was added to the mixture, thoroughly mixed and placed on a thermocycler at 65 °C for 16–48 h and then maintained at 4 °C for less than 24 h. Using a two-step magnetic beads purification, probe excess was removed in PrepStation and target/probe complexes were bound on the cartridge. The data were collected by the digital analyzer (NanoString nCounter® Digital Analyzer) with images of immobilized fluorescent reporters in the sample cartridge. Results of barcode reads were analyzed by nSolver™ Analysis Software 4.0, and differential expression analysis was done with a custom R script.

The NanoString data were analyzed using ROSALIND, a cloud-based software pipeline supported by NanoString for analysis of nCounter data. Comparisons between SKM and saline, and SKM and non-injected groups were analyzed for each timepoint, with addition of covariate analysis for assay run data as necessary. Data were visualized with volcano plots using the EnhancedVolcano package in R.

5.5.3. Bulk RNA sequencing

Purified mRNA was analyzed using a TapeStation 2200 with a high-sensitivity RNA ScreenTape. After the RNA-integrity number (RIN) was confirmed to be adequate, the RNA was processed using the Illumina Stranded mRNA kit. Libraries were quantified via a Qubit 3.0 and fragment size was determined using a TapeStation 2200 with a D5000 ScreenTape. Libraries were then sequenced on a NextSeq 2000 at depth of 75 × 2. Differential expression analysis was done using the Bioconductor DESeq2 pipeline.

5.6. Histological characterization at early timepoints post-injection

5.6.1. Hematoxylin & eosin staining of early timepoint tissues

Two weeks after partial glossectomy injury, either 300 μL of SKM or saline was injected into the injury site. At 3 and 7 days post-injection, tongue tissues were harvested and cryosectioned. Tissue sections were stained with hematoxylin & eosin to assess area of injury, defined by hypercellularity and muscle damage. The area of injury was outlined and normalized to the total tissue area for the section; this percentage of injured area was then compared between groups.

5.6.2. Quantification of arteriole density

Tissue sections from 7 days post-injection for SKM and saline groups were stained against an anti-αSMA antibody and anti-isolectin B4 as previously described (Section 5.4.3). One tissue section was assessed per animal, chosen as the most injured section defined by greatest cellularity. Arteriole density was defined as number of arterioles normalized by the total tissue area, and was statistically compared between groups with an unpaired *t*-test. Furthermore, the distribution of arteriole lumen areas between groups was compared.

5.6.3. Immunohistochemical staining of fibroadipogenic progenitors and developing myofibers

To assess FAP localization in the context of scar area, myofibers, and SKM bolus, an anti-PDGFRα antibody (R&D Systems, Minneapolis, MN, 1:100) with Alexa Fluor™ 568 secondary (Invitrogen, Carlsbad, California, 1:500) was used alongside an anti-collagen I antibody (AF488 secondary), anti-α-sarcoglycan antibody (AF647 secondary), and DAPI as previously described. To assess new and developing myofibers, an anti-embryonic myosin heavy chain antibody (Developmental Studies Hybridoma Bank, Iowa City, Iowa, 1:200) with Alexa Fluor™ 488 secondary was used alongside an anti-α-sarcoglycan antibody (AF568 secondary) and DAPI as previously described. Tissue sections were visualized using an Olympus VS200 fluorescent microscope. To assess density of FAPs within the injured area, which was defined as the region demonstrating disrupted muscle and hypercellularity, the QuPath positive cell detection tool was used to detect cells and define a positive cell as one containing PDGFRα signal within the cytoplasm area of a cell. The number of PDGFRα$^+$ cells was normalized by the total number of nuclei within the injured area.

5.7. Statistical analysis

The initial SKM dosing study was a pilot study that did not aim to achieve statistically significant differences, so n = 2 animals per injection volume were used for this initial investigation. For the investigation of histomorphological changes following SKM injection, sample size was based on a previous study of SKM for muscle regeneration in a model of hindlimb ischemia [17]; using G*Power, 6 animals/group were needed to achieve 90 % power and a significance of 0.05. For gene expression studies, preliminary data with qRT-PCR were used to calculate the sample size; 11 animals/group/timepoint were necessary to achieve 80 % power and a significance of 0.05. Data that followed a parametric distribution were compared using an unpaired *t*-test, or a one-way analysis of variance followed by Tukey's post hoc pairwise comparisons. Data that did not follow a parametric distribution (skeletal muscle cross-sectional fiber area, arteriole lumen area) were analyzed by a Mann-Whitney test [18]. Data were analyzed using GraphPad Prism v8.0, San Diego, CA. Gene expression normalization and differential expression was analyzed using the ROSALIND pipeline, with a fold-change cutoff of 1.2 and p-value cutoff of 0.05. For bulk RNA sequencing, differentially expressed genes were identified as average absolute logFC >0.6 and adjusted p-value <0.1.

Ethics approval and consent to participate

All procedures were approved by the Institutional Animal Care and Use Committee at the University of California, San Diego and conducted according to guidelines set by the American Association for Accreditation of Laboratory Animal Care.

CRediT authorship contribution statement

Emma I. Zelus: Conceptualization, Data curation, Formal analysis, Investigation, Methodology, Project administration, Validation, Visualization, Writing – original draft, Writing – review & editing. **Aaron Panduro:** Data curation. **Isha Deshmukh:** Data curation. **Jacqueline Grime:** Data curation. **Marianna Alperin:** Resources, Supervision, Writing – review & editing. **Andrew M. Vahabzadeh-Hagh:** Conceptualization, Funding acquisition, Methodology, Project administration, Resources, Supervision, Writing – review & editing. **Karen L. Christman:** Conceptualization, Funding acquisition, Methodology, Resources,

Supervision, Writing – review & editing.

Declaration of competing interest

Dr. Christman is a co-founder, board member, consultant, and holds equity interest in VentrixBio, Inc. and Karios Technologies, Inc.

Acknowledgements

Funding provided by the UCSD Galvanizing Engineering in Medicine Program. The authors would like to thank the UC San Diego Stem Cell Genomics Core at the Sanford Consortium for Regenerative Medicine for assistance with RNA sequencing and analysis.

Appendix A. Supplementary data

Supplementary data to this article can be found online at https://doi.org/10.1016/j.bioactmat.2024.05.001.

References

[1] S. Dellis, S. Papadopoulou, K. Krikonis, F. Zigras, J. Frailt. Sarcopenia Fall. (2018).
[2] B. R. Pauloski, n.d., DOI 10.1016/j.pmr.2008.05.010.
[3] P. García-Peris, L. Parón, C. Velasco, C. de la Cuerda, M. Camblor, I. Bretón, H. Herencia, J. Verdaguer, C. Navarro, P. Clave, Clin. Nutr. 26 (2007) 710.
[4] K. Hyo Choi, Y. Ri Son, T. Gyun Kim, Ann. Rehabilit. Med. Orig. Artic. 39 (2015) 210.
[5] N.P. Nguyen, C.C. Moltz, C. Frank, P. Vos, H.J. Smith, U. Karlsson, S. Dutta, F. A. Midyett, J. Barloon, S. Sallah, Ann. Oncol. 15 (2004) 383.
[6] S.E. Langmore, J.M. Pisegna, Int. J. Speech Lang. Pathol. 17 (2015) 222.
[7] E.K. Tran, K.O. Juarez, J.L. Long, World J. Stem Cell. 12 (2020) 1001.
[8] A. M. Vahabzadeh-Hagh, A. N. Goel, J. W. Frederick, G. S. Berke, J. L. Long, 2018, DOI 10.1002/lio2.202..
[9] N. Nativ-Zeltzer, M. A. Kuhn, L. Evangelista, J. D. Anderson, J. A. Nolta, ; D Gregory, E. Canestrari, R. J. Jankowski, P. C. Belafsky, 2021, DOI 10.1002/lary.29606..
[10] M.T. Spang, K.L. Christman, Acta Biomater. 68 (2018) 1.
[11] N. Rao, G. Agmon, M.T. Tierney, J.L. Ungerleider, R.L. Braden, A. Sacco, K. L. Christman, ACS Nano 11 (2017) 3851.
[12] S.B. Seif-Naraghi, J.M. Singelyn, M.A. Salvatore, K.G. Osborn, J.J. Wang, U. Sampat, O.L. Kwan, G.M. Strachan, J. Wong, P.J. Schup-Magoffin, et al., Sci. Transl. Med. 5 (2013), 173ra25 LP.
[13] Z.M. Nezhad, A. Poncelet, L. De Kerchove, P. Gianello, C. Fervaille, G. El Khoury, Z. Mosala Nezhad) (2016), https://doi.org/10.1093/icvts/ivw020.
[14] T.L. Sarrafian, S.C. Bodine, B. Murphy, J.K. Grayson, S.M. Stover, Vet. Surg. 47 (2018) 524.
[15] J.H. Traverse, T.D. Henry, N. Dib, A.N. Patel, C. Pepine, G.L. Schaer, J.A. DeQuach, A.M. Kinsey, P. Chamberlin, K.L. Christman, JACC Basic Transl. Sci. 4 (2019) 659.
[16] J.A. DeQuach, J.E. Lin, C. Cam, D. Hu, M.A. Salvatore, F. Sheikh, K.L. Christman, Eur. Cell. Mater. 23 (2013) 400.
[17] J.L. Ungerleider, T.D. Johnson, M.J. Hernandez, D.I. Elhag, R.L. Braden, M. Dzieciatkowska, K.G. Osborn, K.C. Hansen, E. Mahmud, K.L. Christman, JACC Basic Transl. Sci. 1 (2016) 32.
[18] P. Duran, F.B. Sesillo, L. Burnett, S.A. Menefee, M. Cook, G. Zazueta-Damian, M. Dzieciatkowska, E. Do, S. French, M.M. Shah, et al., bioRxiv 2021 (2021), 05.28.446170.
[19] M.J. Hernandez, E.I. Zelus, M.T. Spang, R.L. Braden, K.L. Christman, Biomater. Sci. 8 (2020) 3511.
[20] H. Lu, D. Huang, R.M. Ransohoff, L. Zhou, Faseb. J. 25 (2011) 3344.
[21] C.A. Reichel, M. Rehberg, M. Lerchenberger, N. Berberich, P. Bihari, A. G. Khandoga, S. Zahler, F. Krombach, Arterioscler. Thromb. Vasc. Biol. 29 (2009) 1787.
[22] B. Deng, M. Wehling-Henricks, S.A. Villalta, Y. Wang, J.G. Tidball, J. Immunol. 189 (2012) 3669.
[23] X. Kang, M.Y. Yang, Y.X. Shi, M.M. Xie, M. Zhu, X.L. Zheng, C.K. Zhang, Z.L. Ge, X. T. Bian, J.T. Lv, et al., Cell Commun. Signal. 16 (2018) 1.
[24] W. Kuswanto, D. Burzyn, M. Panduro, K.K. Wang, Y.C. Jang, A.J. Wagers, C. Benoist, D. Mathis, Immunity 44 (2016) 355.
[25] T. Varga, R. Mounier, A. Patsalos, P. Gogolák, M. Peloquin, A. Horvath, A. Pap, B. Daniel, G. Nagy, E. Pintye, et al., 2016, DOI 10.1016/j.immuni.2016.10.016..
[26] M.P. Alfaro, D.L. Deskins, M. Wallus, J. Dasgupta, J.M. Davidson, L.B. Nanney, M. A. Guney, M. Gannon, P.P. Young, Lab. Invest. 93 (2012) 81.
[27] H.S. Alameddine, J.E. Morgan, J. Neuromuscul. Dis. 3 (2016) 455.
[28] D. Coletti, J.J. Mccarthy, B.M. Scicchitano, C. Mozzetta, L. Madaro, B. Biferali, D. Proietti (2019), https://doi.org/10.3389/fphys.2019.01074.
[29] M.N. Wosczyna, A.A. Biswas, C.A. Cogswell, D.J. Goldhamer, J. Bone Miner. Res. 27 (2012) 1004.
[30] D. Hardy, A. Besnard, M. Latil, G. Jouvion, D. Briand, C. Thépenier, Q. Pascal, A. Guguin, B. Gayraud-Morel, J.-M. Cavaillon, et al., 2016, DOI 10.1371/journal.pone.0147198..
[31] M.D. Diaz, E. Tran, M. Spang, R. Wang, R. Gaetani, C.G. Luo, R. Braden, R.C. Hill, K.C. Hansen, A.N. DeMaria, et al., JACC Basic Transl. Sci. 1 (2021).
[32] B.M. Sicari, J.L. Dziki, B.F. Siu, C.J. Medberry, C.L. Dearth, S.F. Badylak, Biomaterials 35 (2014) 8605.
[33] L.T. Saldin, M.C. Cramer, S.S. Velankar, L.J. White, S.F. Badylak, Acta Biomater. 49 (2017) 1.
[34] W. Yang, P. Hu, J. Orthop. Translat. 13 (2018) 25.
[35] W. Kuswanto, D. Burzyn, M. Panduro, K.K. Wang, Y.C. Jang, A.J. Wagers, C. Benoist, D. Mathis, Immunity 44 (2016) 355.
[36] B. Biferali, D. Proietti, C. Mozzetta, L. Madaro, Front. Physiol. 10 (2019) 1074.
[37] X. Kang, M.Y. Yang, Y.X. Shi, M.M. Xie, M. Zhu, X.L. Zheng, C.K. Zhang, Z.L. Ge, X. T. Bian, J.T. Lv, et al., Cell Commun. Signal. 16 (2018), https://doi.org/10.1186/S12964-018-0251-0.
[38] M.J. Hernandez, E.I. Zelus, M.T. Spang, R.L. Braden, K.L. Christman, Biomater. Sci. 8 (2020) 3511.
[39] J.L. Ungerleider, T.D. Johnson, N. Rao, K.L. Christman, Methods 84 (2015) 53.
[40] Oral Cavity & Oropharyngeal Cancer Key Statistics, 2021. https://www.cancer.org/cancer/oral-cavity-and-oropharyngeal-cancer/about/key-statistics.html.